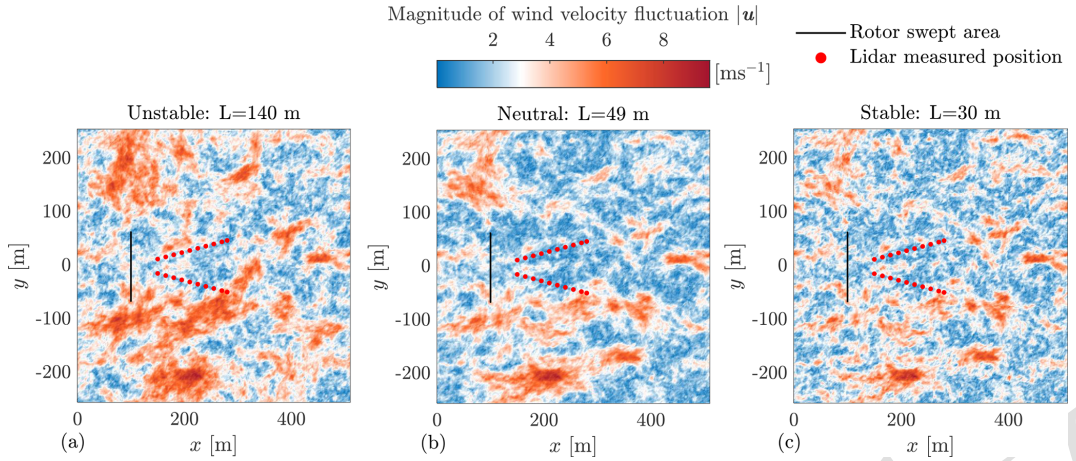

Figure 1. Top view of a turbulence field showing the eddy structures under different atmospheric stability, simulated using the *4D Mann Turbulence Generator* with parameters listed in Table 1. The lidar measured positions are plotted based on a typical four-beam pulsed lidar. The rotor-swept area is drawn based on the NREL 5.0 MW reference wind turbine which has a rotor diameter of 126 m. The length scales L are chosen based on studies by Peña (2019) and Guo et al. (2022a).

where b_1 and b_2 are two constants standing for the slopes of τ in logarithmic scale. Instead of using the hypergeometric function, Guo et al. (2022a) proposed another equation for the eddy lifetime

$$\tau(\mathbf{k}) = \Gamma\left(\frac{\mathrm{d}U}{\mathrm{d}z}\right)^{-1}\left[a(|\mathbf{k}|L)^{b_1}\left((|\mathbf{k}|L)^{10}+1\right)^{\frac{b_2-b_1}{10}}\right], \quad (6)$$

$$\text{with } a = \left[{}_2F_1\left(\frac{1}{3},\frac{17}{6};\frac{4}{3};-1\right)\right]^{-\frac{1}{2}}, \quad (7)$$

which is straightforward to adjust the slopes of the eddy lifetime. They found that adjusting the slope constant b_1 for stable atmospheric stability tends to give better agreements of spectra and coherence between the model and the measurements from a lidar and a meteorological mast. We will use Eq. (6) for the rest of this paper.

The one-dimensional (along the longitudinal wavenumber) cross-spectra of all velocity components with separations Δy and Δz can be obtained by

$$F_{ij}(k_1,\Delta y,\Delta z) = \int \mathbf{\Phi}_{ij}(\mathbf{k})\exp(\mathrm{i}(k_2\Delta y + k_3\Delta z))\mathrm{d}\mathbf{k}_\perp, \quad (8)$$

where $\int \mathrm{d}\mathbf{k}_\perp \equiv \int_{-\infty}^{\infty}\int_{-\infty}^{\infty}\mathrm{d}k_2\mathrm{d}k_3$. Specifically, when $i=j$ and $\Delta y = \Delta z = 0$, it becomes the auto-spectrum of one velocity component at one point, usually written as $F_{ii}(k_1)$. The magnitude-squared coherence between two points in the same yz plane is often interesting, which can be calculated by (Mann, 1994)

$$\mathrm{coh}^2_{ij}(k_1,\Delta y,\Delta z) = \frac{|F_{ij}(k_1,\Delta y,\Delta z)|^2}{F_{ii}(k_1)F_{jj}(k_1)}. \quad (9)$$

And the yz plane co-coherence and quad-coherence are defined by

$$\mathrm{cocoh}_{ij}(k_1,\Delta y,\Delta z) = \frac{\Re(F_{ij}(k_1,\Delta y,\Delta z))}{\sqrt{F_{ii}(k_1)F_{jj}(k_1)}}, \quad (10)$$

and

$$\mathrm{quadcoh}_{ij}(k_1,\Delta y,\Delta z) = \frac{\Im(F_{ij}(k_1,\Delta y,\Delta z))}{\sqrt{F_{ii}(k_1)F_{jj}(k_1)}}, \quad (11)$$

where $\Re$ and $\Im$ are the real and imaginary number operators, respectively.

2.2 Kaimal spectra and exponential coherence model

The Kaimal model given by IEC 61400-1:2019 (2019) uses the following formula to determine the auto-spectra of velocity components:

$$S_i(f) = \frac{4\sigma_i^2\frac{L_i}{U_{\mathrm{ref}}}}{(1+6f\frac{L_i}{U_{\mathrm{ref}}})^{5/3}}, \quad (12)$$

where f is the frequency, L_i is the integral length scale, σ_i is the standard deviation, and U_{ref} is the reference wind speed equivalent to hub-height mean wind speed. The coherence (with square) of the u components of two points in the yz plane is described as

$$\gamma^2_{yz}(\Delta yz, f) = \exp\left(-2a_{yz}r\sqrt{\left(\frac{f}{V_{\mathrm{hub}}}\right)^2+\left(\frac{0.12}{L_c}\right)^2}\right), \quad (13)$$

with $\Delta yz = \sqrt{\Delta y^2+\Delta z^2}$ the separation distance, a_{yz} the coherence decay constant, and L_c the coherence scale parameter. Note that the coherence without square is used in

IEC 61400-1:2019 (2019). The yz plane coherence for the v and w components is not given by the IEC 61400-1:2019 (2019), and they are ignored in this work.

2.3 Modeling of turbulence evolution

The turbulence evolution refers to the phenomenon that the eddy structure changes when the turbulence propagates from upstream to downstream. It is often represented using longitudinal coherence.

2.3.1 Extending the Mann model to include evolution

A space–time tensor that extends the three-dimensional Mann spectral tensor $\mathbf{\Phi}$ to count for the temporal evolution of the turbulence field has been proposed by Guo et al. (2022a). The space–time tensor is evaluated to provide good agreements on the turbulence spectra and coherence including the spectra of all velocity components and the coherence with longitudinal, vertical–lateral, and all combined spatial separations. The validation has been made using data[TS4] from a pulsed lidar and a meteorological mast. Details of the model validation can be found in the work by Guo et al. (2022a). The space–time tensor is written as

$$\Theta_{ij}(\mathbf{k}, \Delta t) = \exp\left(-\frac{\Delta t}{\tau_e(\mathbf{k})}\right)\Phi_{ij}(\mathbf{k}), \tag{14}$$

which defines the ensemble average

$$\Theta_{ij}(\mathbf{k}, \Delta t)\delta(\mathbf{k}-\mathbf{k}') = \langle \hat{u}_i{}^*(\mathbf{k}, t_0)\hat{u}_j(\mathbf{k}', t_0+\Delta t)\rangle, \tag{15}$$

where $\hat{u}_j(\mathbf{k}', t_0+\Delta t)$ denotes the Fourier coefficients of the turbulence field at time $t_0+\Delta t$. τ_e is another eddy lifetime (different from τ) that defines the temporal evolution of the turbulence field. The expression

$$\tau_e(\mathbf{k}) = \gamma\left[a(|\mathbf{k}|L)^{-1}\left((|\mathbf{k}|L)^{10}+1\right)^{-\frac{2}{15}}\right] \tag{16}$$

was found to predicts the longitudinal coherence well as investigated by Guo et al. (2022a). Here, γ is a parameter that determines the strength of turbulence evolution.

In the space–time tensor, the turbulence field is assumed to travel with a mean reference wind speed U_{ref}. After time Δt, the field moves downstream in the positive x direction by $U_{\text{ref}}\Delta t$. Thus, for two points with a longitudinal separation of Δx, the longitudinal coherence (magnitude-squared) of u component can be calculated from

$$\text{coh}^2_{11}(k_1, \Delta x) = \frac{|\int \Theta_{11}(\mathbf{k}, \Delta x/U_{\text{ref}})\mathrm{d}\mathbf{k}_\perp|^2}{F_{11}(k_1)F_{11}(k_1)}, \tag{17}$$

where

$$F_{11}(k_1) = \int \Phi_{11}(\mathbf{k})\mathrm{d}\mathbf{k}_\perp \tag{18}$$

is the auto-spectrum of u component. In practice, the wavenumber-based spectra or coherence is converted to the frequency-based ones using conversion $k_1 = 2\pi f/U_{\text{ref}}$, assuming Taylor (1938)'s frozen hypothesis.

2.3.2 Exponential longitudinal coherence model

On the other hand, Simley and Pao (2015) adjusted the exponential coherence model listed in the IEC 61400-1:2019 (2019) by replacing the transverse and vertical separations with longitudinal separations, which gives the following expression for the longitudinal coherence

$$\gamma_x^2(\Delta x, f) = \exp\left(-a_x\Delta x\sqrt{\left(\frac{f}{U_{\text{ref}}}\right)^2 + b_x^2}\right), \tag{19}$$

where a_x and b_x are two parameters, and f is the frequency. Specifically, a_x determines the decay effect of the coherence, and b_x determines the intercept (value at 0 frequency) (Chen et al., 2021). Simley and Pao (2015) validated Eq. (19) using large eddy simulations (LESs) of different atmospheric stability classes. Besides, Davoust and von Terzi (2016) and Chen et al. (2021) verified the exponential evolution model using lidar measurement, showing that the expression by Simley and Pao (2015) agrees well with the measurement. In their study, they found possible a_x and b_x by fitting the coherence calculated from measurement data to the model. As a result, $0 < a_x < 6$ was observed, and b_x was found in the order of magnitude $\leq 10^{-3}$.

To include the exponential longitudinal coherence model into the analysis of lidar measurement correlation, a general "direct product" approach is used to combine the lateral-vertical coherence and the longitudinal coherence (Laks et al., 2013; Simley, 2015; Bossanyi et al., 2014; Schlipf et al., 2013a), which means the overall coherence

$$\gamma_{xyz}(f) = \gamma_{yz}(f)\cdot\gamma_x(f). \tag{20}$$

As shown by Chen et al. (2022), the direct product approach allows an efficient algorithm to generate the Kaimal-model-based 4D stochastic turbulence field using statically independent 3D turbulence fields using *evoTurb*.

2.4 Turbulence under different atmospheric stability classes

Atmospheric stability indicates the buoyancy effect on the turbulence generation, and it is usually related to the temperature gradient by height. It is interesting to investigate its impact on the filter design of LAC since the turbine will experience different atmospheric stability conditions during operation. The filter is necessary to filter out the uncorrelated frequencies in the REWS estimated by lidar, as will be discussed later in Sect. 3. In the rest of this paper, we use the Mann turbulence parameter sets representative of unstable,

neutral, and stable conditions based on the study by Peña (2019) and Guo et al. (2022a), as listed in Table 1. It is worth mentioning that the $\alpha\varepsilon^{2/3}$ parameter is scaled such that the TI corresponds to the IEC 61400-1:2019 (2019) class 1A definition. Actually, the turbulence intensity is related to the atmospheric conditions. Usually, TI is generally high in unstable stability, moderate in neutral stability, and low in stable stability (Peña et al., 2017). In this work, we emphasize analyzing the impact of turbulence length scale and anisotropy on turbine loads and LAC benefits. Therefore, the same TI level is assumed for the three stability classes. This assumption tends to be not realistic, but it helps to identify the impact of length scale on turbine load, as later analyzed in Sect. 5.2.

As for the Kaimal model, we chose the parameters listed by the IEC 61400-1:2019 (2019) for the neutral stability because these parameters were already found to give similar spectra and coherence compared to the Mann model with neutral stability parameters. Also, keeping these parameters allows readers to compare the results with those from existing literature, e.g., Schlipf (2015), Simley et al. (2018), and Dong et al. (2021). For unstable and stable stability classes, we fit the Kaimal spectra by CE2 the Mann-model-based spectra using the following optimization process: TS5

$$\min_{L_i,\sigma_i} \sum_{n=1}^{N} \left[\frac{1}{k_{1,n}} \left(S_i(f_n) \cdot f_n - 2F_{ii}(k_{1,n}) \cdot k_{1,n} \right)^2 \right], \quad \text{s.t. } k_{1,n} = \frac{2\pi f_n}{U_{\text{ref}}} \text{ and } i = 1, 2, 3. \tag{21}$$

Here, n is the index of the discrete frequency vector f_n and wavenumber TS6 vector $k_{1,n}$, and N is the size of the discrete vector CE3. Note that the Mann model spectra $F_{ii}(k_{1,n})$ are multiplied by 2 since they are the two-sided spectra, while the Kaimal spectra are single-sided. Similarly, we fit the yz plane exponential coherence for the Kaimal model by the Mann model using

$$\min_{a_{yz},L_c} \sum_{n=1}^{N} \left[\frac{1}{k_{1,n}} \left(\gamma_{yz}(f_n) - \text{cocoh}_{11}(k_{1,n}, \Delta y, \Delta z) \right)^2 \right], \quad \text{s.t. } k_{1,n} = \frac{2\pi f_n}{U_{\text{ref}}} \text{ and } \Delta y = \Delta z = 20\,\text{m}, \tag{22}$$

where the fitting uses the co-coherence and ignores the quad-coherence. We fit the co-coherence instead of the magnitude-squared coherence, because the exponential coherence model (Eqs. 13 and 19) only includes the real co-coherence, whereas the coherence of the Mann model includes both co-coherence and quad-coherence. The medium separation $\Delta y = \Delta z = 20\,\text{m}$ has been chosen for the optimization problem. For both optimization equations, the squared error in each discrete vector is divided by $k_{1,n}$ to ensure equivalent weighting of the optimization function at a different frequency or wavenumber ranges. The fitted spectra and yz plane coherence are shown by Fig. 2a and b, and the turbulence parameters are summarized in Table 1.

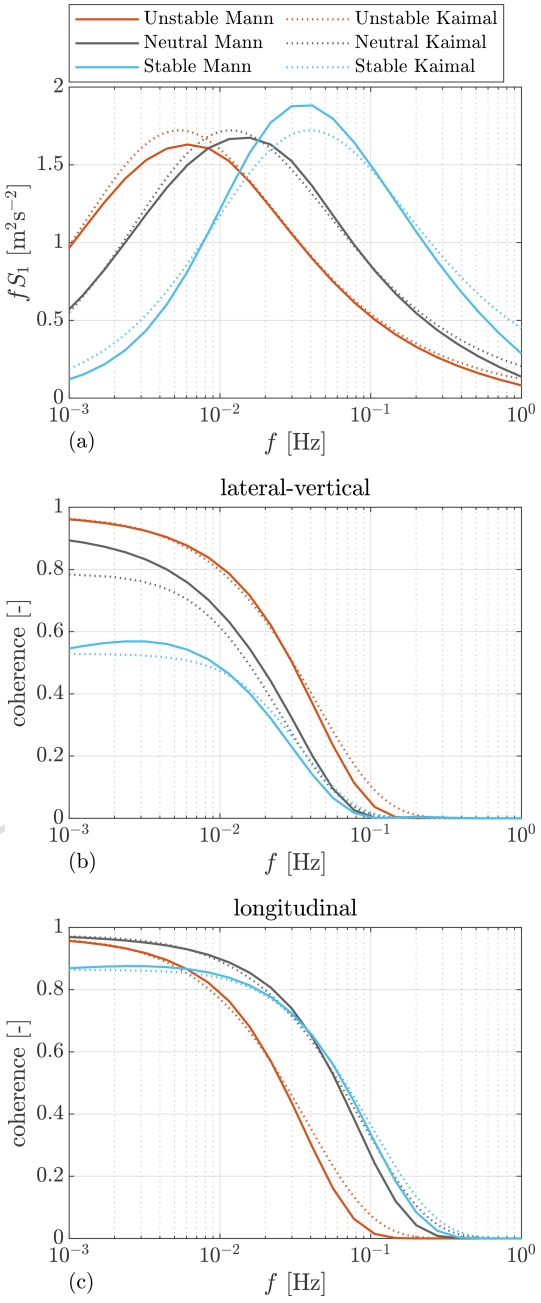

Figure 2. **(a)** The auto-spectra of the longitudinal velocity component under different stability classes. **(b)** Lateral–vertical coherence of the longitudinal velocity component calculated using the Mann spectral tensor and fitted by the exponential coherence model. Note the co-coherence is shown for the Mann spectral tensor. **(c)** Longitudinal coherence of the longitudinal velocity component calculated using the space–time tensor and fitted by the exponential coherence model. The results are calculated with a mean wind speed of 16 ms^{-1}.